Supplement of Clim. Past, 21, 753–772, 2025
https://doi.org/10.5194/cp-21-753-2025-supplement

Supplement of

Environmental controls of rapid terrestrial organic matter mobilization to the western Laptev Sea since the Last Deglaciation

Tsai-Wen Lin et al.

Correspondence to: Tsai-Wen Lin (tsai-wen.lin@awi.de) and Gesine Mollenhauer (gesine.mollenhauer@awi.de)

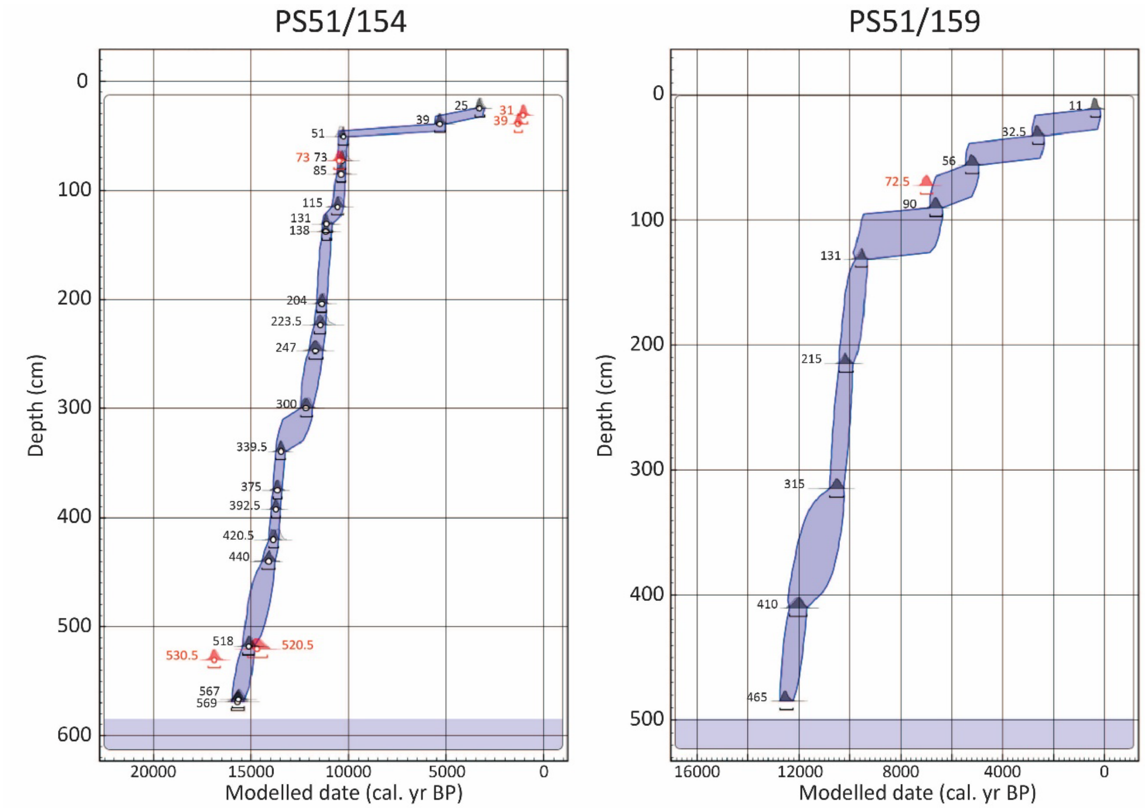

Fig S1. Age-depth models for cores PS51/154 and PS51/159. The two models are calculated by Oxcal 4.4 software (Bronk Ramsey, 2021), with Marine20 calibration curve (Heaton et al., 2020) and ΔR = −95 ± 61 yr, according to the Laptev Sea reservoir age reconstruction from Bauch et al. (2001). The numbers next to the age probabilities denote the depth of the sample. Samples marked in red indicate the samples excluded from age model determination. The purple bands indicate the range of 95.4% age probability.

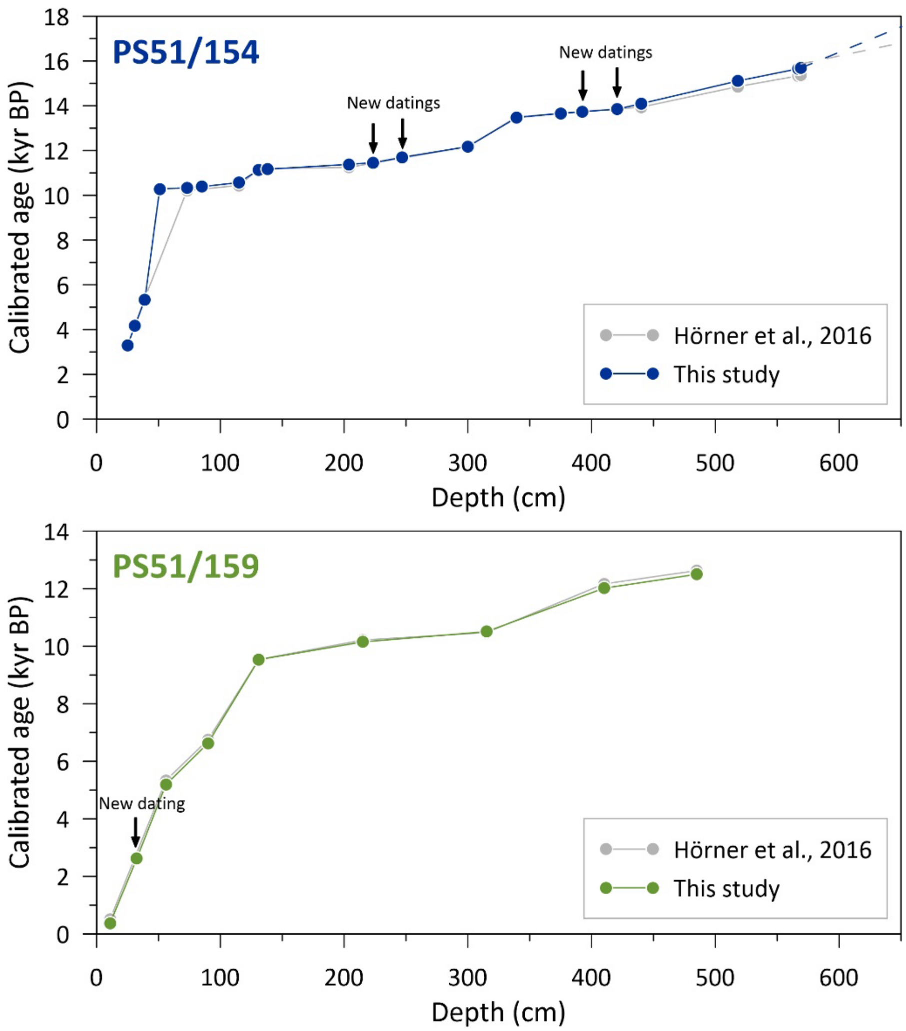

Fig S2. Age-depth models of core PS51/154 and PS51/159 published in Hörner et al. (2016) (grey lines) and in this study (colored lines). Black arrows indicate the new radiocarbon dating results added in this study (see Table 1). The dashed lines at the bottom of the core PS51/154 indicate the age model extrapolated from the radiocarbon dating points.

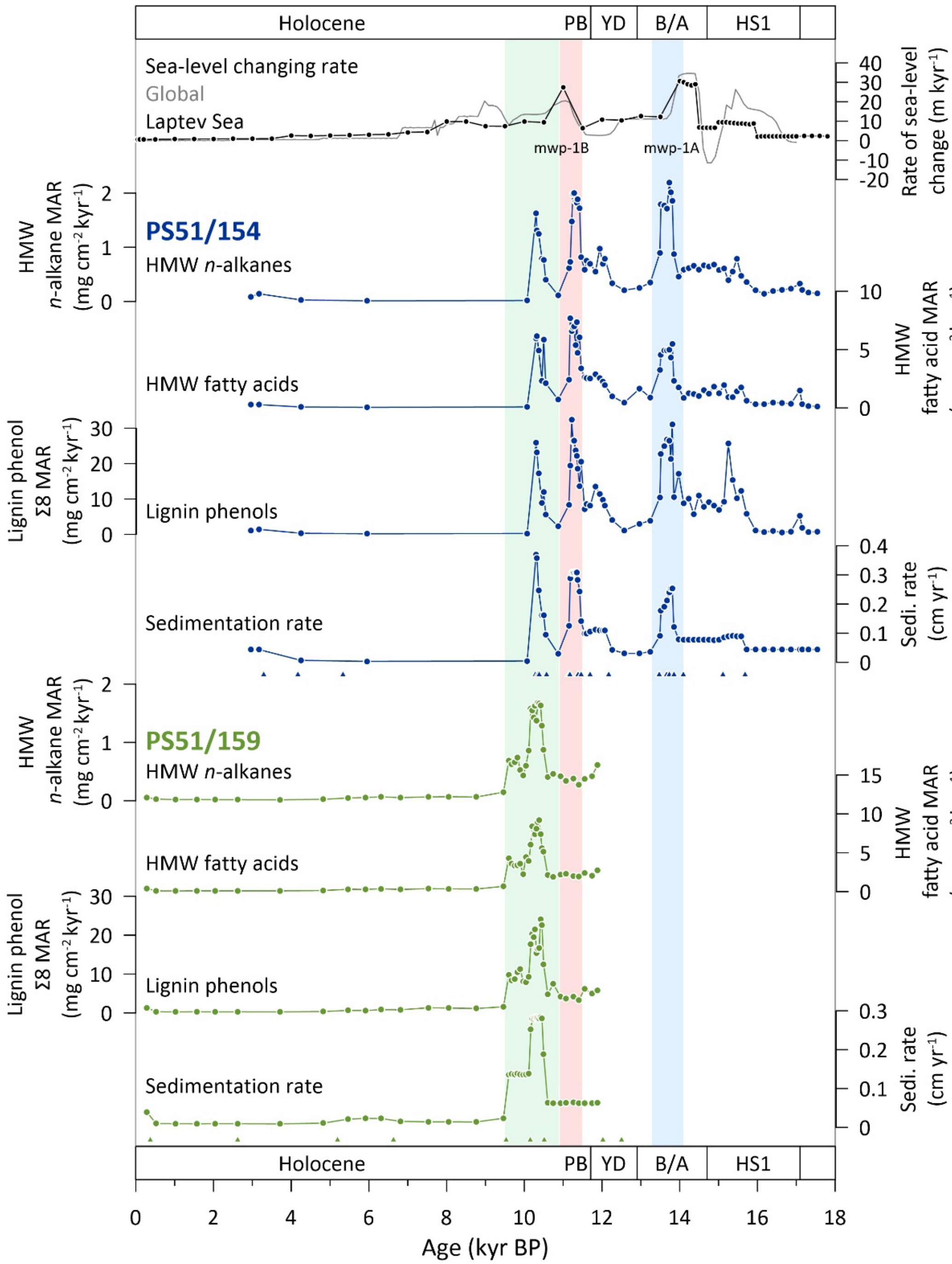

Fig S3. Terrestrial biomarker mass accumulation rates (MAR) from high molecular weight (HMW) *n*-alkanes, HMW fatty acids, and lignin phenols in cores PS51/154 (dark blue, this study) and PS51/159 (light green, this study) as well as sedimentation rates from the two cores. The compounds we used to calculate HMW *n*-alkane MAR include *n*-C_{27}, *n*-C_{29}, *n*-C_{31}, and *n*-C_{33}, and HMW fatty acid MAR includes *n*-$C_{24:0}$, *n*-$C_{26:0}$, *n*-$C_{28:0}$, and *n*-$C_{30:0}$. For lignin phenol MAR, we used the sum of Vl, Vn, Vd, Sl, Sn, Sd, *p*Cd, and Fd (Σ8). The triangles denote the age points from radiocarbon dating measurements. The color bars highlight the periods with HMW fatty acid MAR peaks from 14.1 to 13.2 kyr BP (blue, terrOM MAR peak I), from 11.6 to 10.9 kyr BP (red, terrOM MAR peak II), and from 10.9 to 9.5 kyr BP (green, terrOM MAR peak III). Meltwater pulses are denoted as mwp-1A and mwp-1B. The names of different paleoclimate periods are indicated by acronyms (HS1: Heinrich Stadial 1, B/A: Bølling-Allerød, YD: Younger Dryas, PB: Preboreal).

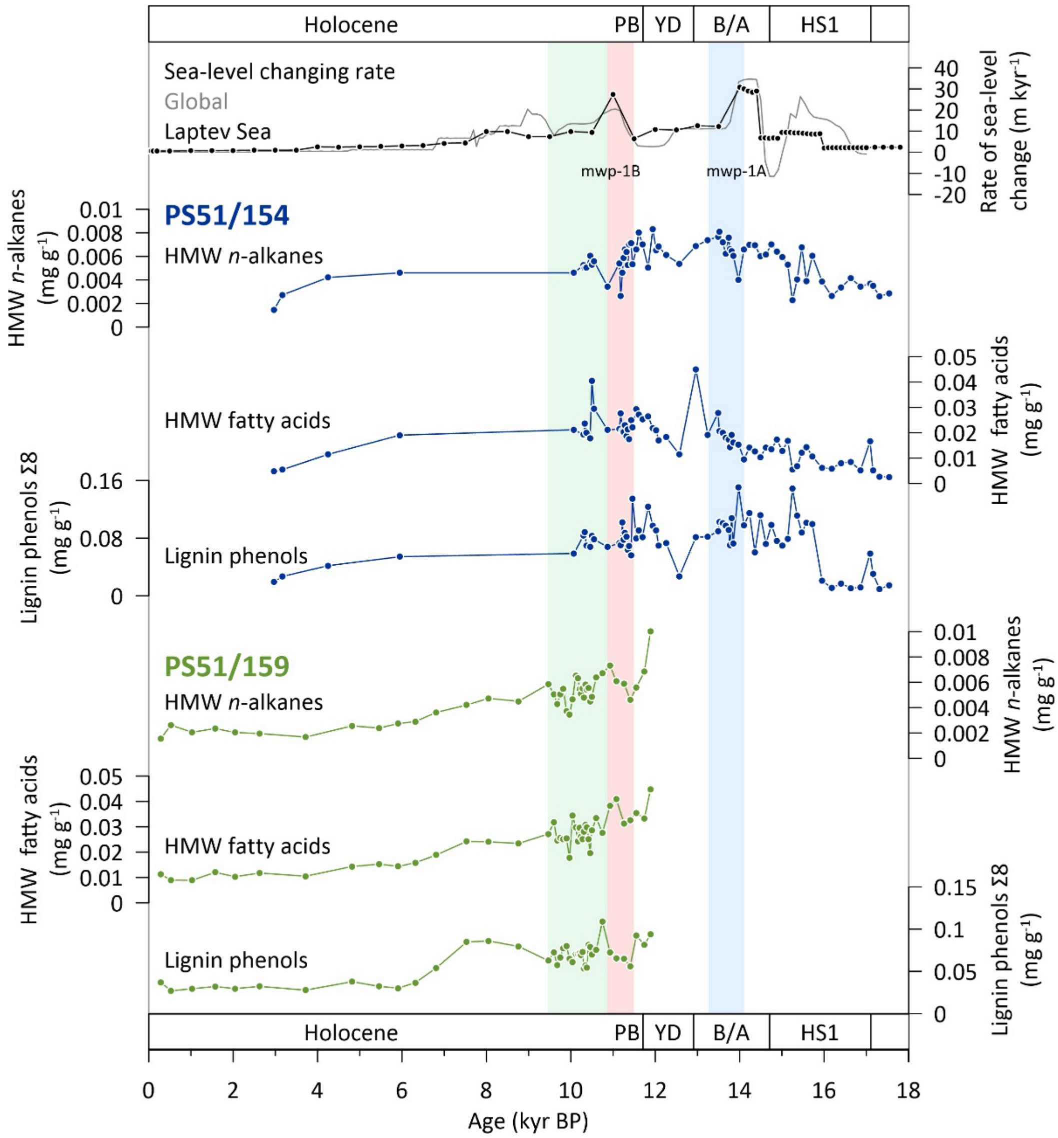

Fig S4. Terrestrial biomarker contents from HMW *n*-alkanes, HMW fatty acids, and lignin phenols in cores PS51/154 (dark blue, this study) and PS51/159 (light green, this study). The global sea-level changing rate is labeled in light gray (Lambeck et al., 2014), and the sea-level changing rate in the western Laptev Sea is labeled in black (Klemann et al., 2015). The color bars highlight the periods with HMW fatty acid MAR peaks from 14.1 to 13.2 kyr BP (blue, terrOM MAR peak I), from 11.6 to 10.9 kyr BP (red, terrOM MAR peak II), and from 10.9 to 9.5 kyr BP (green, terrOM MAR peak III). Meltwater pulses are denoted as mwp-1A and mwp-1B. The names of different paleoclimate periods are indicated by acronyms (HS1: Heinrich Stadial 1, B/A: Bølling-Allerød, YD: Younger Dryas, PB: Preboreal).

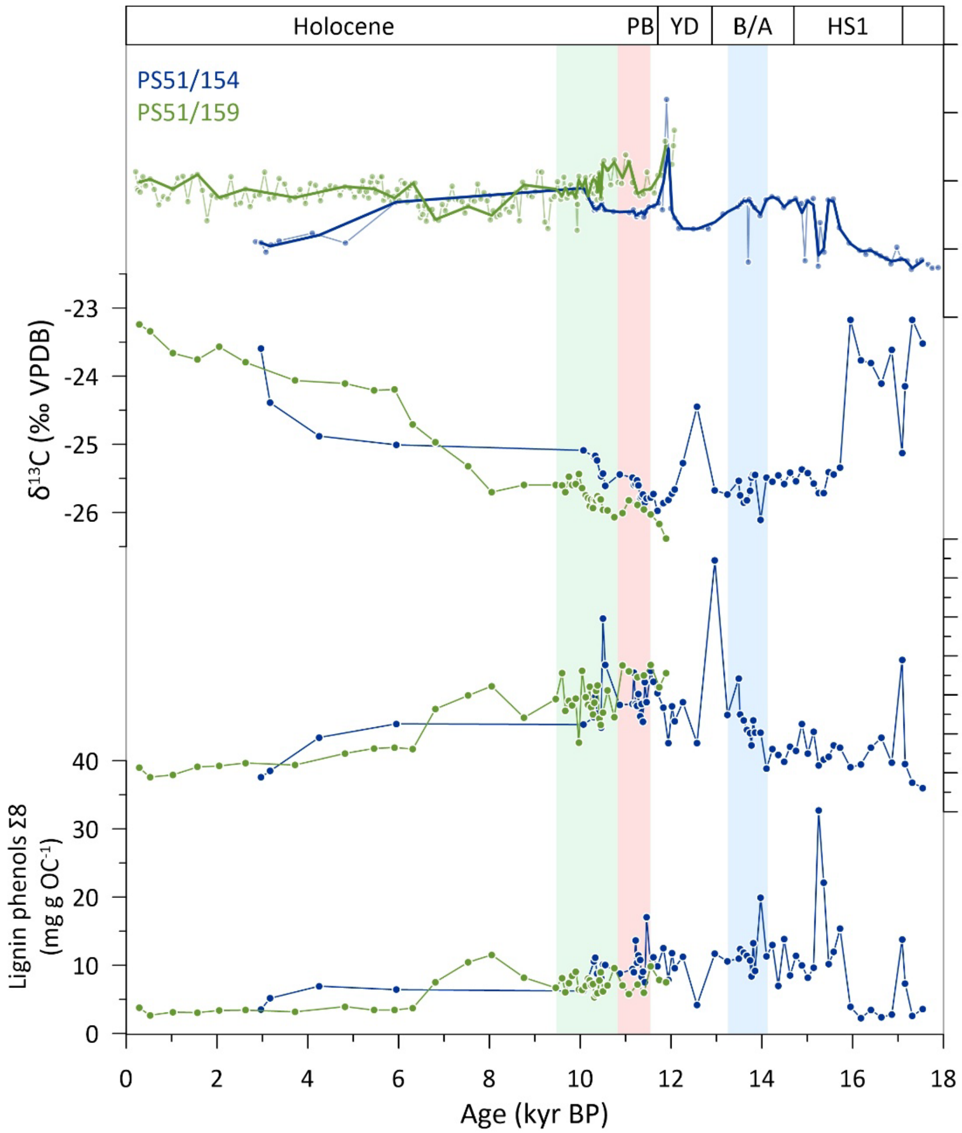

Fig S5. TOC (Hörner et al., 2016), $\delta^{13}C$ (this study), HMW fatty acid content (this study), and lignin phenol (Σ8) content (this study) in cores PS51/154 and PS51/159. The thick lines in TOC show the interpolated value at the same sampling resolution as the other measurements. The color bars highlight the periods with HMW fatty acid MAR peaks from 14.1 to 13.2 kyr BP (blue, terrOM MAR peak I), from 11.6 to 10.9 kyr BP (red, terrOM MAR peak II), and from 10.9 to 9.5 kyr BP (green, terrOM MAR peak III). The names of different paleoclimate periods are indicated by acronyms (HS1: Heinrich Stadial 1, B/A: Bølling-Allerød, YD: Younger Dryas, PB: Preboreal).

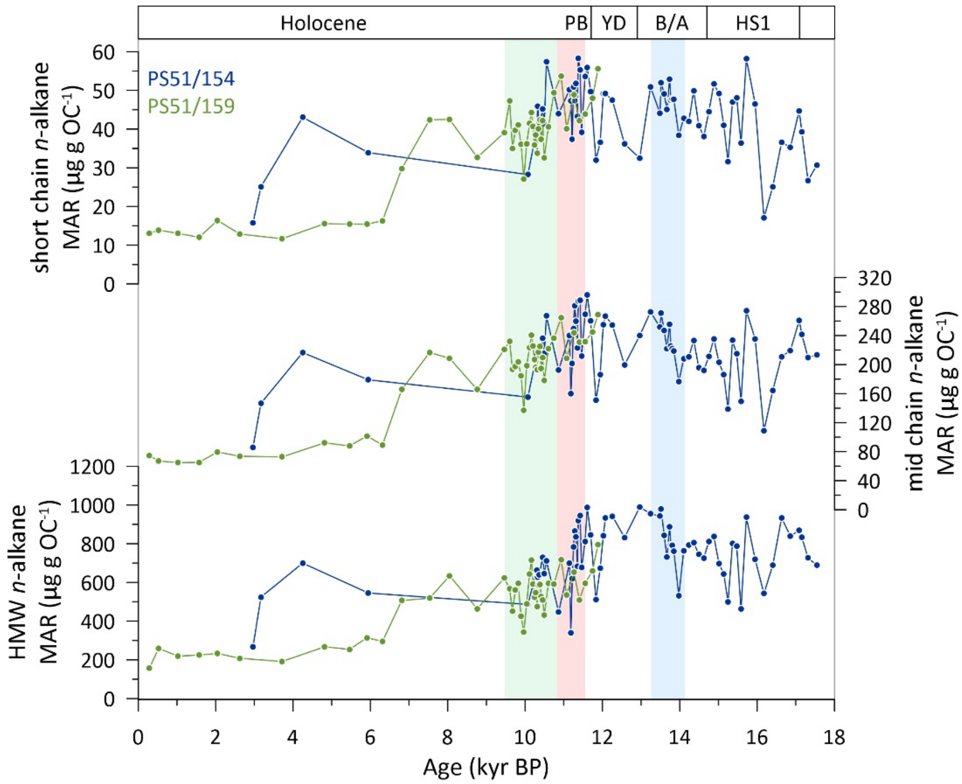

Fig S6. Contents of short-chain, mid-chain, and long-chain (HMW) *n*-alkanes in cores PS51/154 (dark blue) and PS51/159 (light green). Colored bars highlight periods of HMW fatty acid MAR peaks: from 14.1 to 13.2 kyr BP (blue, terrOM MAR peak I), from 11.6 to 10.9 kyr BP (red, terrOM MAR peak II), and from 10.9 to 9.5 kyr BP (green, terrOM MAR peak III). The primary source of short chain n-alkanes is marine primary production, while the mid-chain *n*-alkanes are found abundant in peatland or aquatic plants, and the primary source of long-chain (HMW) *n*-alkanes are higher plants (Bianchi and Canuel, 2011).

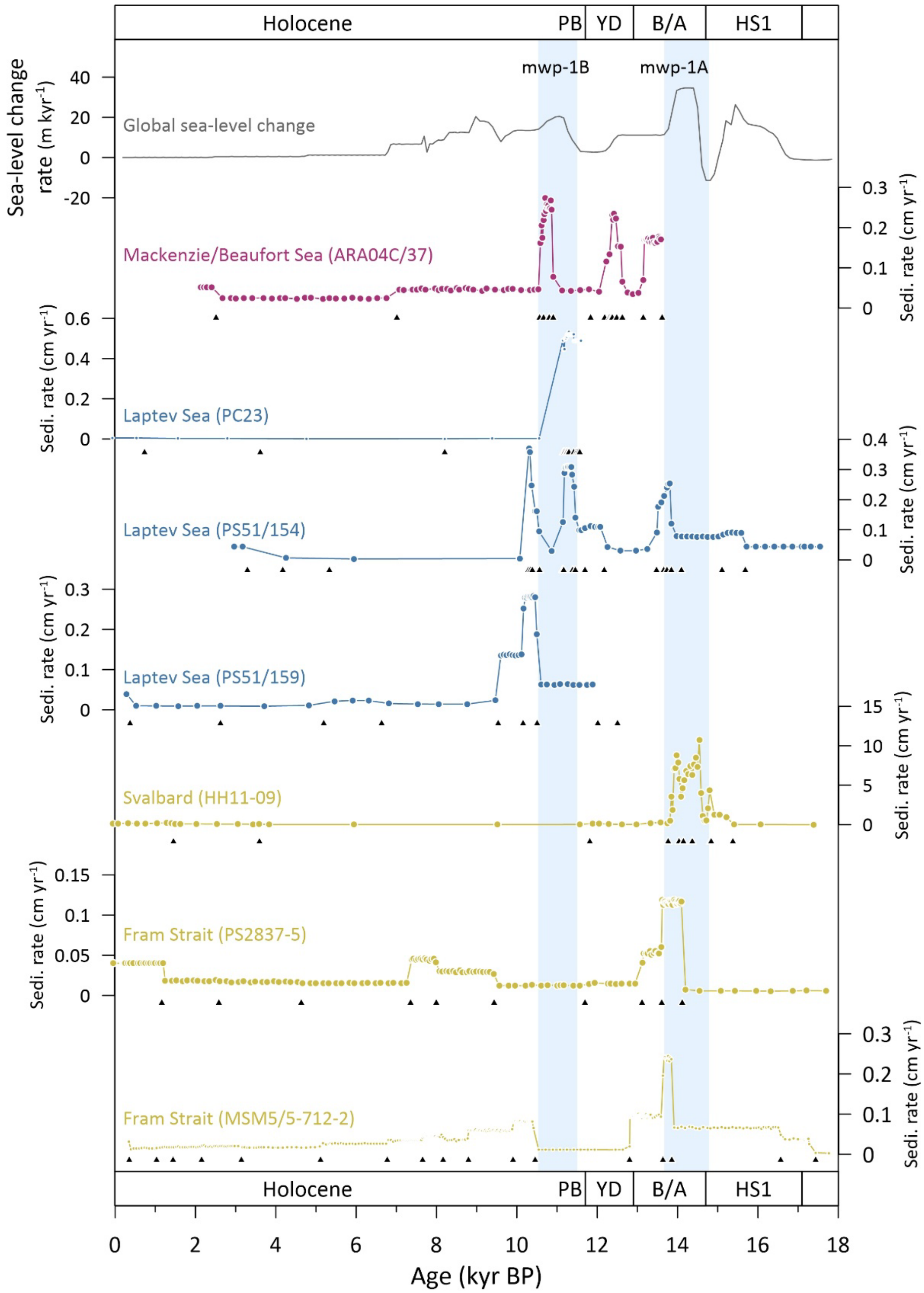

Fig S7. Rate of global sea-level change (Lambeck et al., 2014) and sedimentation rate changes of cores ARA04C/37, Beaufort Sea (Wu et al., 2020); PC23, Laptev Sea (Tesi et al., 2016); PS51/154, Laptev Sea (this study); PS51/159, Laptev Sea (this study); HH11-09, northern Svalbard continental margin (Nogarotto et al., 2023); PS2837-5, Fram Strait (Birgel and Hass, 2004); MSM05/5-712-2, Fram Strait (Müller and Stein, 2014; Aagaard-Sørensen et al., 2014; Zamelczyk et al., 2014). Black triangles under each records indicates the controlling points for age-depth models. The blue bars highlight the period of rapid sea-level rise. Meltwater pulses are denoted as mwp-1A and mwp-1B. The names of different paleoclimate periods are indicated by acronyms (HS1: Heinrich Stadial 1, B/A: Bølling-Allerød, YD: Younger Dryas, PB: Preboreal).

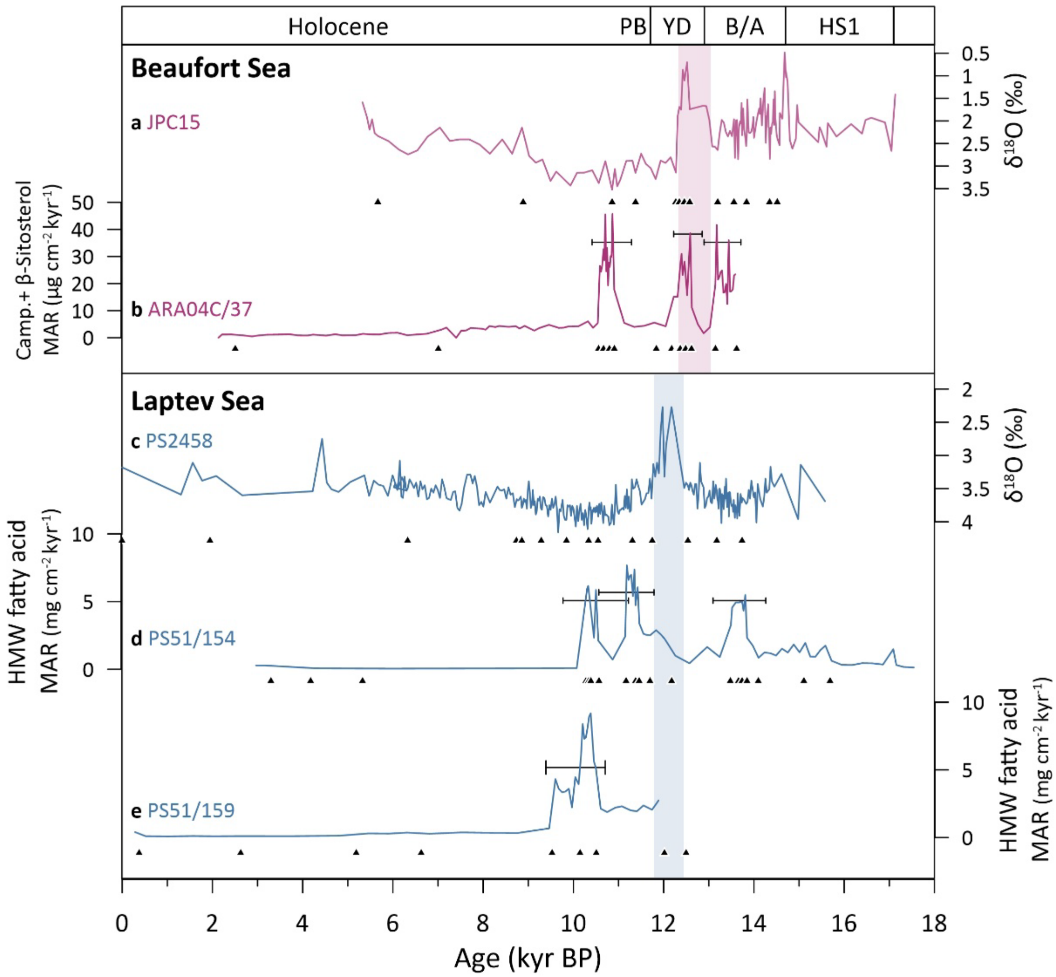

Fig S8. Comparison of freshwater event and terrestrial organic matter (terrOM) mass accumulation rate (MAR) in the Beaufort Sea: (a) δ^{18}O values of *Neogloboquadrina pachyderma* from core JPC15 (Keigwin et al., 2018). (b) Campestreol + β-sitosterol MAR from core ARA04C/37 (Wu et al., 2020). Laptev Sea: (c) δ^{18}O values of *Neogloboquadrina pachyderma* from core PS2458 (Spielhagen et al., 2005). (d) high molecular weight (HMW) fatty acid MAR from core PS51/154 (this study). (e) HMW fatty acid MAR from core PS51/159 (this study). All records were calibrated against Marien20 curve (detail in Table S3). Black triangles denote age control points. Black intervals under MAR peaks indicate age uncertainty ranges. Purple and blue bars highlight freshwater events in the Beaufort Sea and the Laptev Sea, respectively.

Table S1. Sedimentation rate, bulk density, and HMW fatty acid mass accumulation rate (MAR) of core PS51/154. The HMW fatty was calculated by the sum of *n*-$C_{24:0}$, *n*-$C_{26:0}$, *n*-$C_{28:0}$, and *n*-$C_{30:0}$ fatty acids.

Depth (cm)	Age (cal. kyr BP)	Sedimentation rate (cm kyr^{-1})	Dry bulk density (g cm^{-3})	HMW fatty acid MAR (mg kyr^{-1} cm^{-2})
10.5	2.965	43.9	1.35	0.286
19.5	3.170	43.9	1.19	0.285
31.5	4.249	6.87	1.04	0.082
40.5	5.947	3.31	0.84	0.053
50.5	10.073	4.6	0.88	0.085
59.5	10.303	370	0.83	5.952
68.5	10.327	358	0.73	6.162
80.5	10.368	247	1.00	4.926
96.5	10.455	162	0.81	2.332
103.5	10.499	162	0.89	5.862
112	10.551	94.6	0.76	2.121
123.5	10.868	29.5	1.15	0.717
133.5	11.149	126	0.90	2.435
142.5	11.183	288	0.96	7.680
154	11.220	307	1.04	6.595
163.5	11.251	308	1.10	6.893
172.5	11.280	308	0.98	6.974
184.5	11.319	309	0.94	5.400
194.5	11.352	308	1.12	7.369
202	11.376	283	0.95	4.729
214.5	11.425	243	1.00	6.059
223.5	11.460	141	1.08	3.387
232.5	11.551	99.2	0.90	2.624
238	11.607	99.2	0.95	2.555
247	11.697	105	0.94	2.509
262	11.833	112	0.98	2.890
274	11.941	110	1.07	2.560
283	12.023	110	0.98	2.241
289	12.077	110	1.05	1.959
302.5	12.259	43.4	1.27	1.002
312	12.571	30.5	1.27	0.442
324	12.964	30.5	1.20	1.649
332.5	13.243	36.7	1.29	0.905
342	13.488	91.3	1.28	3.252
347.5	13.517	177	1.25	4.558
363	13.598	191	1.29	4.935
377	13.670	212	1.30	4.938
392.5	13.738	240	1.20	5.000
400.5	13.769	253	1.20	4.328

410.5	13.809	254	1.13	5.493
420.5	13.848	121	1.19	2.322
430.5	13.975	78.9	1.44	1.747
440.5	14.102	77.5	1.15	0.848
450.5	14.232	77	1.14	1.242
460.5	14.361	77.3	1.22	1.189
470.5	14.491	76.8	1.28	1.019
480.5	14.622	77	1.40	1.526
490.5	14.751	76.9	1.19	1.239
500.5	14.882	76.7	1.39	1.835
510.5	15.012	78	1.26	1.250
520.5	15.138	84.9	1.36	1.949
530.5	15.249	89.4	1.94	0.936
540.5	15.361	90.9	1.52	0.928
550.5	15.472	89.3	1.30	1.413
560.5	15.584	89.5	1.36	1.751
570.5	15.721	43.9	1.34	0.628
580.5	15.949	43.9	1.21	0.326
590.5	16.177	43.9	1.23	0.317
600.5	16.405	43.9	1.30	0.458
610.5	16.632	43.9	1.18	0.439
620.5	16.860	43.9	1.57	0.353
630.5	17.088	43.9	2.04	1.486
633.5	17.156	43.9	1.41	0.316
640.5	17.316	43.9	1.45	0.173
650.5	17.544	43.9	1.22	0.134

Table S2. Sedimentation rate, bulk density, and HMW fatty acid mass accumulation rate (MAR) of core PS51/159. The HMW fatty was calculated by the sum of *n*-$C_{24:0}$, *n*-$C_{26:0}$, *n*-$C_{28:0}$, and *n*-$C_{30:0}$ fatty acids.

Depth (cm)	Age (cal. kyr BP)	Sedimentation rate (cm kyr^{-1})	Dry bulk density (g cm^{-3})	HMW fatty acid MAR (mg kyr^{-1} cm^{-2})
7.5	0.286	39.1	0.92	0.403
12.5	0.523	10	1.14	0.103
17.5	1.026	9.55	0.99	0.084
22.5	1.573	9.32	1.04	0.116
27	2.046	9.5	0.96	0.094
32.5	2.624	9.51	0.99	0.111
42.5	3.716	8.94	1.09	0.103
52.5	4.819	11	0.91	0.143
62.5	5.460	21.2	0.94	0.305
73	5.910	23.3	0.87	0.292
82.5	6.313	22.9	1.02	0.368
92.5	6.811	15.6	0.96	0.283

102.5	7.532	14.3	1.11	0.383
110	8.049	14.2	1.03	0.353
120	8.763	14.1	1.02	0.336
130	9.463	23.5	1.07	0.683
140	9.601	135	1.01	4.321
150	9.674	137	1.07	3.605
160	9.748	136	0.96	3.353
170	9.821	138	0.98	3.399
180.5	9.897	136	1.04	3.608
190	9.968	135	0.93	2.231
200	10.041	136	0.95	4.464
210	10.115	138	0.96	3.944
219.5	10.167	252	0.99	6.036
230	10.206	279	1.02	8.394
240	10.241	279	1.00	7.302
250	10.277	282	1.04	7.395
260	10.312	282	1.02	8.097
270	10.348	281	1.03	8.930
280	10.383	280	1.10	9.177
290	10.419	283	1.04	7.420
300	10.454	280	1.02	5.619
312	10.497	188	0.95	5.137
321	10.603	63	1.01	2.138
330	10.747	62.7	1.09	1.885
341.5	10.930	62.3	0.93	2.214
350.5	11.074	63.5	0.89	2.310
362.5	11.263	64	1.01	2.016
371.5	11.404	62.3	0.95	1.939
380.5	11.552	62.4	1.07	2.373
392.5	11.742	62	1.00	2.058
401.5	11.887	63.2	0.97	2.743

Table S3. Comparison of previous calibration and updating calibration methods on the core used in this study.

Core ID	Reference of previous age model	Previous calibration curve	Previous R or ΔR (yr)	Updated ΔR for Marine20 (yr)	Method to updated ΔR
ARA04C/37 JPC15	Keigwin et al. (2018); Wu et al. (2022)	Marine13	ΔR = 200 ± 100 during younger dryas, 0 ± 100 for the other periods	Variable ΔR, ΔR = 50 ± 100 during younger dryas, ΔR= −150 ± 100 for the other periods	Update ΔR from Keigwin et al. (2018) by minus 150 year (Heaton et al., 2023)
PC23	Tesi et al. (2016)	Marine13 for marine samples /IntCal13 for plant samples	ΔR = 400 during early Holocene, 67 during mid and late Holocene	ΔR = 411 ± 56 during early Holocene, ΔR = −95 ± 91 during mid and late Holocene	Adopted from Sabino et al. (2024)
PS51/154	Taldenkova et al. (2010)	Fairbanks 0107	R = 370, constant	ΔR = −95 ± 61	From Marine20 database, average of 5 adjacent available datapoints
PS51/159	Taldenkova et al. (2010)	Fairbanks 0107	R = 370, constant	ΔR = −95 ± 61	From Marine20 database, average of 5 adjacent available datapoints
HH11-09	Nogarotto et al. (2023)	Marine20	Variable ΔR between each datapoints	Variable ΔR	Adopted from Nogarotto et al. (2023)
PS2837-5	Nørgaard-Pedersen et al. (2003)	CALIB 4.1.2	R = 0 ± 400, constant	ΔR = −41 ± 30	From Marine20 database, average of 10 adjacent available datapoints
MSM5/5-712-2	Müller and Stein (2014); Aagaard-Sørensen et al. (2014); Zamelczyk et al. (2014)	Marine09	ΔR = 151 ± 51, constant	ΔR = −65 ± 33	From Marine20 database, average of 7 adjacent available datapoints (distance <620 km)
PS2458	Nicolas et al. (2024)	Marine20	ΔR = 345 ± 60, constant	ΔR = 345 ± 60, constant	Adopted from Nicolas et al. (2024)

References

Aagaard-Sørensen, S., Husum, K., Werner, K., Spielhagen, R. F., Hald, M., and Marchitto, T. M.: A Late Glacial–Early Holocene multiproxy record from the eastern Fram Strait, Polar North Atlantic, Marine Geology, 355, 15-26, 10.1016/j.margeo.2014.05.009, 2014.

Bauch, H. A., Mueller-Lupp, T., Taldenkova, E., Spielhagen, R. F., Kassens, H., Grootes, P. M., Thiede, J., Heinemeier, J., and Petryashov, V.: Chronology of the Holocene transgression at the North Siberian margin, Global Planetary Change, 31, 125-139, 2001.

Bianchi, T. S. and Canuel, E. A.: Chemical biomarkers in aquatic ecosystems, in: Chemical Biomarkers in Aquatic Ecosystems, Princeton University Press, 2011.
Birgel, D. and Hass, H.: Oceanic and atmospheric variations during the last deglaciation in the Fram Strait (Arctic Ocean): a coupled high-resolution organic-geochemical and sedimentological study, Quaternary Science Reviews, 23, 29-47, 10.1016/j.quascirev.2003.10.001, 2004.
Heaton, T. J., Bard, E., Bronk Ramsey, C., Butzin, M., Hatté, C., Hughen, K. A., Köhler, P., and Reimer, P. J.: A Response to Community Questions on the Marine20 Radiocarbon Age Calibration Curve: Marine Reservoir Ages and the Calibration of 14c Samples from the Oceans, Radiocarbon, 65, 247-273, 10.1017/rdc.2022.66, 2023.
Heaton, T. J., Köhler, P., Butzin, M., Bard, E., Reimer, R. W., Austin, W. E. N., Bronk Ramsey, C., Grootes, P. M., Hughen, K. A., Kromer, B., Reimer, P. J., Adkins, J., Burke, A., Cook, M. S., Olsen, J., and Skinner, L. C.: Marine20—The Marine Radiocarbon Age Calibration Curve (0–55,000 cal BP), Radiocarbon, 62, 779-820, 10.1017/rdc.2020.68, 2020.
Hörner, T., Stein, R., Fahl, K., and Birgel, D.: Post-glacial variability of sea ice cover, river run-off and biological production in the western Laptev Sea (Arctic Ocean)–A high-resolution biomarker study, Quaternary Science Reviews, 143, 133-149, 2016.
Keigwin, L. D., Klotsko, S., Zhao, N., Reilly, B., Giosan, L., and Driscoll, N. W.: Deglacial floods in the Beaufort Sea preceded Younger Dryas cooling, Nature Geoscience, 11, 599-604, 10.1038/s41561-018-0169-6, 2018.
Klemann, V., Heim, B., Bauch, H. A., Wetterich, S., and Opel, T.: Sea-level evolution of the Laptev Sea and the East Siberian Sea since the last glacial maximum, Arktos, 1, 10.1007/s41063-015-0004-x, 2015.
Lambeck, K., Rouby, H., Purcell, A., Sun, Y., and Sambridge, M.: Sea level and global ice volumes from the Last Glacial Maximum to the Holocene, Proceedings of the National Academy of Sciences of the United States of America, 111, 15296-15303, 10.1073/pnas.1411762111, 2014.
Müller, J. and Stein, R.: High-resolution record of late glacial and deglacial sea ice changes in Fram Strait corroborates ice–ocean interactions during abrupt climate shifts, Earth and Planetary Science Letters, 403, 446-455, 10.1016/j.epsl.2014.07.016, 2014.
Nicolas, A., Mollenhauer, G., Lachner, J., Stübner, K., Malter, M., Wollenburg, J., Grotheer, H., and Adolphi, F.: Precise dating of deglacial Laptev Sea sediments via 14C and authigenic 10Be/9Be – assessing local 14C reservoir ages, EGUsphere, 2024, 1-19, 10.5194/egusphere-2024-1992, 2024.
Nogarotto, A., Noormets, R., Chauhan, T., Mollenhauer, G., Hefter, J., Grotheer, H., Belt, S., Colleoni, F., Muschitiello, F., Capotondi, L., Pellegrini, C., and Tesi, T.: Coastal permafrost was massively eroded during the Bølling-Allerød warm period, Communications Earth & Environment, 4, 350, https://doi.org/10.1038/s43247-023-01013-y, 2023.
Nørgaard-Pedersen, N., Spielhagen, R. F., Erlenkeuser, H., Grootes, P. M., Heinemeier, J., and Knies, J.: Arctic Ocean during the Last Glacial Maximum: Atlantic and polar domains of surface water mass distribution and ice cover, Paleoceanography, 18, n/a-n/a, 10.1029/2002pa000781, 2003.

Sabino, M., Gustafsson, Ö., Wild, B., Semiletov, I. P., Dudarev, O. V., Ingrosso, G., and Tesi, T.: Feedbacks From Young Permafrost Carbon Remobilization to the Deglacial Methane Rise, Global Biogeochemical Cycles, 38, 10.1029/2024gb008164, 2024.

Spielhagen, R., Erlenkeuser, H., and Siegert, C.: History of freshwater runoff across the Laptev Sea (Arctic) during the last deglaciation, Global and Planetary Change, 48, 187-207, 10.1016/j.gloplacha.2004.12.013, 2005.

Taldenkova, E., Bauch, H. A., Gottschalk, J., Nikolaev, S., Rostovtseva, Y., Pogodina, I., Ovsepyan, Y., and Kandiano, E.: History of ice-rafting and water mass evolution at the northern Siberian continental margin (Laptev Sea) during Late Glacial and Holocene times, Quaternary Science Reviews, 29, 3919-3935, 2010.

Tesi, T., Muschitiello, F., Smittenberg, R. H., Jakobsson, M., Vonk, J. E., Hill, P., Andersson, A., Kirchner, N., Noormets, R., Dudarev, O., Semiletov, I., and Gustafsson, O.: Massive remobilization of permafrost carbon during post-glacial warming, Nature Communications, 7, 13653, 10.1038/ncomms13653, 2016.

Wu, J., Stein, R., Fahl, K., Syring, N., Nam, S.-I., Hefter, J., Mollenhauer, G., and Geibert, W.: Deglacial to Holocene variability in surface water characteristics and major floods in the Beaufort Sea, Communications Earth & Environment, 1, 10.1038/s43247-020-00028-z, 2020.

Wu, J., Mollenhauer, G., Stein, R., Kohler, P., Hefter, J., Fahl, K., Grotheer, H., Wei, B., and Nam, S. I.: Deglacial release of petrogenic and permafrost carbon from the Canadian Arctic impacting the carbon cycle, Nature Communications, 13, 7172, 10.1038/s41467-022-34725-4, 2022.

Zamelczyk, K., Rasmussen, T. L., Husum, K., Godtliebsen, F., and Hald, M.: Surface water conditions and calcium carbonate preservation in the Fram Strait during marine isotope stage 2, 28.8–15.4 kyr, Paleoceanography, 29, 1-12, 2014.